JOURNAL OF APPLIED PHYSICS **115**, 043514 (2014)

Modified InGaN/GaN quantum wells with dual-wavelength green-yellow emission

Z. L. Fang,[1,a)] Q. F. Li,[1] X. Y. Shen,[1] H. Xiong,[1] J. F. Cai,[1] J. Y. Kang,[1] and W. Z. Shen[2]
[1]*Department of Physics, Xiamen University, Xiamen 361005, People's Republic of China*
[2]*Department of Physics, Shanghai Jiao Tong University, Shanghai 200240, People's Republic of China*

(Received 16 October 2013; accepted 13 January 2014; published online 28 January 2014)

Energy band engineering by indium pretreatment of the bottom GaN barriers and control of the growth temperature profile for the InGaN active layers were employed to improve the green-yellow emitting InGaN/GaN quantum well (QW). The modified InGaN/GaN QWs were investigated by various characterization techniques and demonstrated to be of good interface abruptness and well-defined indium concentration profile, composed of 0.52 nm $In_{0.35}Ga_{0.65}N$ "wetting layer," 1.56 nm $In_{0.35\text{-}0.22}Ga_{0.65\text{-}0.78}N$ graded layers, and 1.56 nm $In_{0.22}Ga_{0.78}N$ layer along the growth direction. Broad-band dual-wavelength green-yellow emission at about 497 and 568 nm was observed and attributed to the major contribution of enhanced interband transitions from the first and second quantized electron states "e1" and "e2" to the first quantized hole state "h1." With the modified QW structure, electron overflow loss would be suppressed by filling of the excited electron state with electrons at high carrier injection density and reduction in polarization-induced band bending. APSYS simulation shows efficiency and droop improvements due to the enhanced overlapping of electron and hole wave functions inside the modified InGaN active layers, and the enhanced interband transitions involving the excited electron state.
[http://dx.doi.org/10.1063/1.4863208]

I. INTRODUCTION

In the past decades, great efforts have been made to improve the materials and structural properties as well as surface/interface qualities, and optical properties of the group-III nitrides.[1–4] With increase of indium content in InGaN active layers for long-wavelength emission, the crystalline quality deteriorates quickly leading to increase of nonradiative recombination rate; moreover, strong strain-induced piezoelectric polarization fields (PFs) enhance the space separation of electrons and holes resulting in decrease of radiative recombination rate. As a result, the internal quantum efficiency (IQE) of green InGaN-based light emitting diodes (LEDs) dramatically drops.[5–8] Furthermore, the IQE decreases with increase of injection current (namely efficiency droop),[9,10] caused by electron overflow loss or carrier leakage due to the PF-induced band bending,[11–14] nonradiative recombination loss including Auger loss and nonradiative recombination at defects,[15,16] and low efficiency of hole injection.[17] Low IQE and efficiency droop for the InGaN-based green LEDs have become great obstacles for commercial applications of red-green-blue (RGB) color-mixed LEDs in solid state lighting.[5]

Various methods have been employed to improve the crystalline qualities as well as to overcome the negative effects of PFs on the IQE and efficiency droop of the InGaN-based materials and devices.[18–34] For instance, surface modification of GaN films has been applied to improve the interface quality, growth behavior, and luminescence properties of InGaN/GaN quantum wells (QWs).[18,19] Si-doped GaN barriers are usually employed for PF screening but with blocking effect on hole transport.[20] PF reduction has also been realized by using ternary InGaN barriers or quaternary AlGaInN barriers with appropriate chemical components.[21,22] Growth on nonpolar and semipolar planes has been carried out for reducing the PF within the InGaN QWs along the growth direction.[23–27] Recently, energy band engineering by growth of complex active layer structures has attracted intense research interest and was employed to reduce the PF-induced band bending for enhancement of the overlapping of electron and hole wave functions.[28–34] In this study, a novel modified InGaN active layer structure composed of high indium content InGaN "wetting layers," graded InGaN layers (so-called triangular QW with a gradual decrease of indium content, as distinct from the rectangular QW of constant indium content in the InGaN active layers), and relatively low indium content InGaN layers was grown and investigated in detail. The luminescence properties and mechanism were characterized and analyzed experimentally and theoretically. With the modified active layer structure, a decrease in PF-induced band bending and enhanced interband transitions are expected. Green-yellow emission efficiency and droop improvements may be achieved for the modified InGaN/GaN QWs. Details are discussed as follows.

II. EXPERIMENTAL AND THEORETICAL METHODS

A. Epitaxy

The metalorganic vapor phase epitaxy of GaN films and InGaN/GaN QWs was carried out on c-sapphire substrates. Trimethylgallium (TMGa), Trimethylindium (TMIn), and high-purity ammonia were used as the source precursors and silane as the n-type dopant. First, the sapphire substrates were cleaned at 1060 °C and 100 Torr for 15 min in H_2 ambient

[a)]Electronic mail: zhilaifang@hotmail.com

followed by nitridation at 550 °C for 4 min. A conventional 25 nm low-temperature GaN nucleation layer was grown at 535 °C and 500 Torr followed by a high-temperature annealing process.[35] The subsequent growth of $\sim$1.6 μm thick GaN epilayers was carried out at 1035 °C and 100 Torr with TMGa/NH_3 ratio gradually increasing from low to high. During the growth of wells and barriers, nitrogen was used as the carrier gas, whereas hydrogen was used as the carrier gas in the other growth stages. Slightly Si-doped ($\sim 1 \times 10^{18}$ cm^{-2}) GaN barriers were grown at 786 °C. The barrier surface was pretreated by a TMIn flow (200 sccm) over the surface at 670 °C for 10 s. A high indium content InGaN "wetting layer" would be formed by the pretreatment. This was followed by the growth of a graded InGaN layer at temperature ramping from 670 to 697 °C. After then a relatively low indium content InGaN layer was continuously grown at 697 °C. Before temperature ramping for the growth of high-temperature barrier layers at 786 °C, a very thin low-temperature GaN layer as a "well protection layer" was grown at 697 °C for suppressing the indium outdiffusion to the barrier layers.[36] The AlGaN electron blocking layer, which was found to reduce the hole injection efficiency at high carrier injection density,[37] was not employed in this study. The indium content and thickness of the InGaN active layers were determined by various characterization techniques and will be addressed later. Bare InGaN layers, GaN capped InGaN layers, and five-period multiple QWs were prepared for studies.

B. Simulation

Crosslight's APSYS, advanced physical models of semiconductor devices, was employed to simulate the physical parameters of the InGaN/GaN QWs.[38] The APSYS simulation software package is based on 2D/3D finite element analysis of electrical, optical, and thermal properties of compound semiconductor devices. The APSYS can deal with optical and electrical properties of the LED devices by solving the Poisson's equation, current continuity equations, carrier transport equation, quantum mechanical wave equation, and photon rate equation. Here, the energy band structure, radiative recombination, and luminescence properties were numerically studied.

C. Characterization

Cross-sectional bright-field transmission electron microscopy (TEM) was employed to characterize the microstructures of the InGaN/GaN QWs. High-resolution X-ray diffraction (HR-XRD) was used to analyze the interface quality, average indium content, and period thickness of the modified InGaN/GaN QWs. X-ray photoelectron spectroscopy (XPS) with an Al K_α X-ray excitation source ($h\nu = 1486.6$ eV) was used to analyze the average indium content of the InGaN active layers. High-angle annular dark field scanning TEM (HAADF-STEM) was applied to further investigate the microstructures of the InGaN/GaN QWs as well as the integrated indium distribution within the InGaN layers. The integrated indium concentration profile along the growth direction for the InGaN active layers was evaluated by the HAADF-STEM analysis combined with the XPS and HR-XRD analysis of the indium content. The photoluminescence (PL) excited by a 325 nm He-Cd laser was measured at 300 K for the modified InGaN/GaN QWs.

III. RESULTS AND DISCUSSION

A. Microstructures and indium concentration profile of the modified InGaN/GaN QWs

Figure 1 shows the cross-sectional bright-field TEM images of the modified InGaN/GaN QWs. The white arrow indicates the growth direction. As shown in Fig. 1(a), abrupt interfaces between the dark-contrast stripes (InGaN) and bright-contrast regions (GaN) were observed. The thickness of the GaN barriers and InGaN QWs is estimated to be about 10.5 nm and 3.5 nm, respectively. Figure 1(b) shows the HR-TEM image of the InGaN QW. Relatively dark contrast was observed at the lower interface (the interface between bottom GaN barrier and InGaN QW) of the modified InGaN layers indicating the formation of relatively high indium content InGaN layers there.

HR-XRD was employed to further investigate the microstructure, interface quality, and average indium content of the InGaN/GaN QWs. Figure 2 shows the XRD ω-2θ scan profile of the (0002) reflection of the modified InGaN/GaN QWs. Well-resolved high order satellite peaks were observed indicating high-quality interfaces between GaN barriers and InGaN QWs achieved. Theoretical fitting of the spectrum was performed by the Panalytical's Epitaxy 4.3a software. In the simulation, the layer structure is composed of 1.60 μm bottom GaN buffer layer, 10.5 nm GaN barrier layers, 3.50 nm $In_{0.26}Ga_{0.74}N$ QW layers, and 50.0 nm GaN cap at top. The simulation curve (red) fits well with the XRD ω-2θ scan profile (black curve) of the modified InGaN/GaN QWs. Accordingly, the average indium content of the InGaN active layers was evaluated to be about 26% with a QW thickness of about 3.5 nm, as consistent with the HR-TEM results.

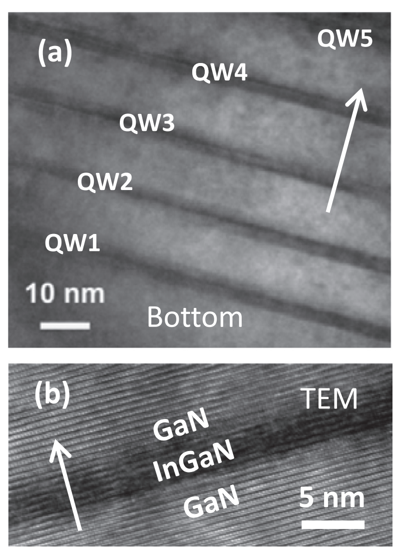

FIG. 1. (a) Cross-sectional bright-field TEM and (b) HR-TEM images of the modified InGaN/GaN QWs. The arrow indicates the growth direction. The bottom QW is numbered as "QW1," whereas the top QW as "QW5."

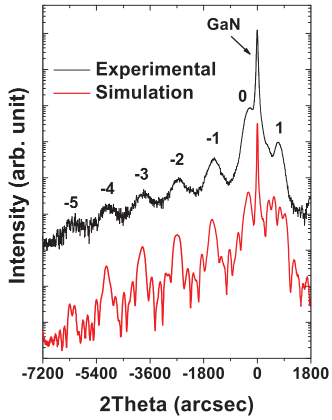

FIG. 2. Experimental and simulated XRD ω-2θ scan profile of the (0002) reflection of the modified InGaN/GaN QWs.

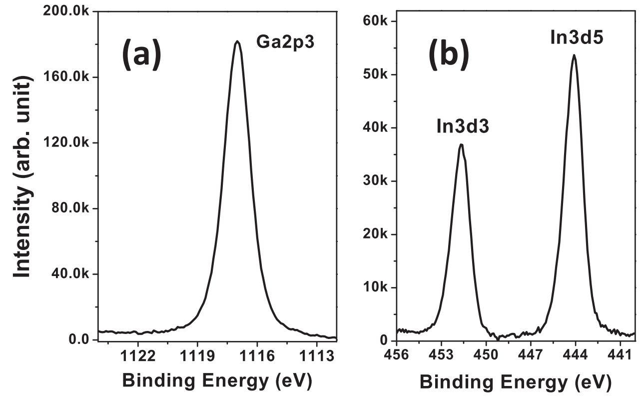

FIG. 3. XPS spectra of the modified InGaN active layers: (a) the Ga2p3 and (b) In3d photoelectron peaks.

XPS, an appropriate technique for investigating the 3.5 nm InGaN active layers due to the detection of photoelectrons arising from within 4 nm of the surface, was employed to analyze the surface chemical compositions of the bare InGaN active layers. The XPS spectra of the Ga2p3 and In3d photoelectron peaks are shown in Figs. 3(a) and 3(b). The Ga2p3 peak locates at $\sim$1117.0 eV, whereas the In3d5 peak at $\sim$444.2 eV. The percentage of the indium composition in the sum of indium and gallium can be estimated by $X_{In} = \frac{I_{In3d5}/F_{In3d5}}{(I_{In3d5}/F_{In3d5}+I_{Ga2p3}/F_{Ga2p3})}$, where I denotes the integrated intensity of the XPS photoelectron peaks and F the sensitivity factors ($F_{Ga2p3} = 2.75$ and $F_{In3d5} = 4.53$). The average indium content in the InGaN layers is estimated to be about 25%, which is consistent with the XRD analysis.

HAADF-STEM was employed to further investigate the modified InGaN layers and to estimate the indium distribution along the growth direction. Figure 4(a) shows an integrated typical HAADF-STEM image of the InGaN/GaN multiple QWs. Due to the higher atomic mass of indium compared with that of gallium, the InGaN layers have a higher intensity and thus depicted brighter than the GaN layers. Accordingly, the narrow bright contrast stripes correspond to the InGaN layers, whereas the wide dark contrast stripes to the GaN barrier layers. Figure 4(b) shows an indium line profile crossing over the InGaN/GaN multiple QWs along the growth direction. Stronger intensity was observed at the lower interface (GaN-to-InGaN) of each modified InGaN QW indicating the incorporation of higher indium content there. At the upper interface (InGaN-to-GaN), there is a tail with weaker intensity compared with that at the lower interface, i.e., the upper interface is of lower indium content and not as abrupt as the lower interface of the InGaN layers. To further investigate the indium concentration profile inside InGaN active layers along the growth direction, high-resolution HAADF-STEM of the modified InGaN/GaN QW was characterized and shown in Fig. 4(c). Atomic rows of the GaN and InGaN layers were observed. The integrated indium concentration profile (after integration of the indium concentration laterally along the InGaN layers) of the InGaN active layers along the growth direction is drawn in Fig. 4(d). The InGaN active layers are composed of

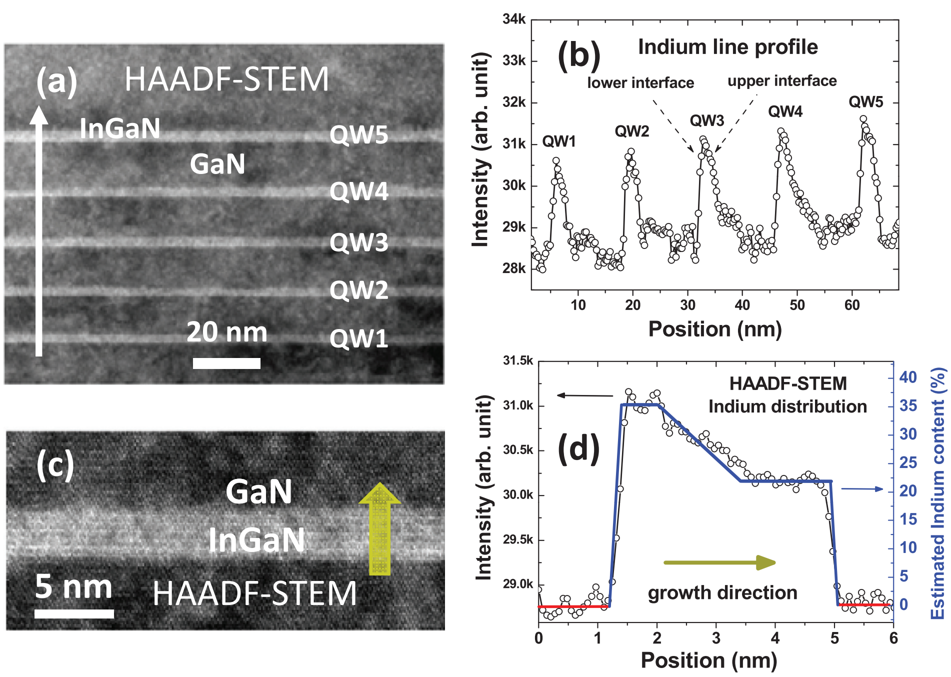

FIG. 4. (a) HAADF-STEM image of the modified InGaN/GaN QWs. The arrow indicates the growth direction. The bottom QW is numbered as "QW1," whereas the top QW as "QW5." (b) Indium line profile of the five-period QWs. (c) HR-STEM image of the modified InGaN/GaN QWs. (d) Integrated indium concentration profile showing the evaluated indium content along the growth direction. The evaluation of the integrated indium concentration profile is based on the average indium content of the InGaN layers as derived from XRD and XPS, and the normalized HAADF-STEM intensity profile after subtraction of the background signal (intensity of the GaN barriers).

relatively high indium content InGaN layers at the lower interface and relatively low indium content InGaN layers (shoulder) at the upper interface. To evaluate the distribution of indium content in the InGaN layers, we assume the HAADF-STEM intensity of the GaN barrier layers (where the indium content is zero) as the background signal, and the calibrated HAADF-STEM intensity (calibration by subtraction of the background signal) linearly dependent on the indium content. Considering that the average indium content of about 26% for the modified InGaN layers as derived from the XRD and XPS analyses, the HAADF-STEM intensity (left axis) in Fig. 4(d) can be converted to the estimated indium content (right axis). As a result, the integrated indium concentration profile of the modified InGaN active layers along the growth direction can be depicted as 0.52 nm high indium content (∼35%) InGaN "wetting layer," 1.56 nm graded InGaN layers (decrease of indium content from ∼35% to ∼22%), and 1.56 nm relatively low indium content (∼22%) InGaN layers, which is consistent with the experimental design of the active layer structure by indium pretreatment and control of the InGaN growth temperature profile. Modified InGaN/GaN QW structure of well-defined indium distribution profile and GaN-InGaN interface abruptness has been demonstrated.

B. Luminescence properties and energy band structures

Figure 5(a) shows the PL spectrum of the modified InGaN/GaN QWs measured at 300 K. Broad-band dual-wavelength green-yellow emission was observed, which may be applicable for monolithic or RGB white light sources. The emission spectrum can be fitted by two peaks at 568 nm ("P1," 2.18 eV) and 497 nm ("P2," 2.49 eV). Dual-wavelength emission was previously observed in thick InGaN layers (>60 nm) and attributed to the significant strain relaxation.[39,40] Without significant strain relaxation for thin InGaN layers, the additional peak disappeared.[39] In this study, thin InGaN layers (3.64 nm) were grown with the lack of significant strain relaxation, as demonstrated by the TEM and XRD investigations. Therefore, the emergence of the additional emission peak was not caused by strain relaxation. Strong lateral fluctuation of indium content in InGaN layers, which was considered as one of the origins for the broad-band emission, would not result in a specific dual-wavelength emission. Furthermore, as investigated by STEM, lateral fluctuation of indium content was not evident for the modified InGaN/GaN QW structure. The vertical variation of indium content along the growth direction was intentionally controlled for energy band engineering and enhanced emission. The origin of the dual-wavelength emission will be further discussed later.

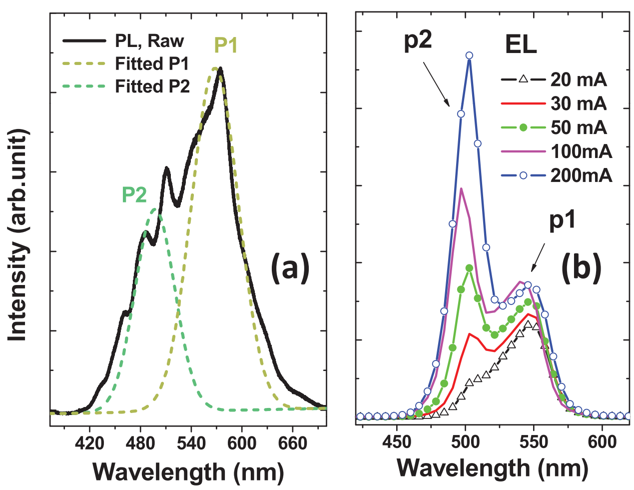

FIG. 5. (a) PL spectrum of the modified QWs measured at 300 K. The QW emission spectrum can be fitted by two peaks at 568 nm ("P1," 2.18 eV) and 497 nm ("P2," 2.49 eV). (b) The simulated EL spectra of the modified QWs under various injection currents. The emission peaks are labeled as "p1" and "p2."

To investigate the evolution of the emission spectra with injection carrier density, electroluminescence (EL) of the modified InGaN/GaN QWs at various injection currents (20, 30, 50, 100, and 200 mA) was numerically studied by APSYS and shown in Fig. 5(b). The simulated InGaN active layer structure is the same as the modified active layer structure, which is composed of 0.52 nm $In_{0.35}Ga_{0.65}N$ "wetting layer," 1.56 nm $In_{0.35\text{-}0.22}Ga_{0.65\text{-}0.78}N$ graded layer, and 1.56 nm $In_{0.22}Ga_{0.78}N$ layer along the growth direction. Similar to the PL spectrum, dual-wavelength emission was observed in the EL spectrum with a relatively narrow full-width-at-half-maximum (FWHM). In the APSYS simulation, the EL spectra were computed on the assumption of a uniform broadening parameter $\Gamma = 20$ meV typical for the conventional III-V compounds,[41] i.e., with a FWHM of about 4-5 nm for the green-yellow emission in the wavelength range of about 500–570 nm. It was reported in the literature that the broadening parameter Γ may increase to as large as about 50–70 meV for the long-wavelength emission,[41] i.e., with a FWHM of about 10–17 nm for the green-yellow emission. Accordingly, it is reasonable that the FWHM of the simulated EL emission peaks is narrower than that of the PL emission peaks in Fig. 5. With the increase of injection current, the luminescence intensity of the emission peak "p1" at about 550 nm (2.25 eV) increases slowly, whereas the luminescence intensity of "p2" at about 502 nm (2.47 eV) increases greatly. Considering that broad-band dual-wavelength emission is not (usually) observed in the PL and EL spectra of the conventional InGaN/GaN QWs of thin InGaN active layer (with significant efficiency droop),[42] the emergence of the additional peak "p2" in EL of the modified InGaN/GaN QWs with significant increase of emission intensity at high carrier concentration suggests an alternative to suppress the efficiency droop.

To further explore the origin of the broad-band dual-wavelength green-yellow emission for the modified InGaN/GaN QWs, APSYS was employed to simulate the physical parameters of the InGaN/GaN QWs. Figure 6(a) shows the energy band diagram and wave functions of the modified QW structure, which is composed of 0.52 nm $In_{0.35}Ga_{0.65}N$ "wetting layer," 1.56 nm $In_{0.35\text{-}0.22}Ga_{0.65\text{-}0.78}N$ graded layer, and 1.56 nm $In_{0.22}Ga_{0.78}N$ layer along the growth direction. For comparisons, a conventional 3.64 nm $In_{0.33\text{-}0.23}Ga_{0.67\text{-}0.77}N$/GaN triangular QW structure (gradual decrease of indium content from 33% to 23% within the

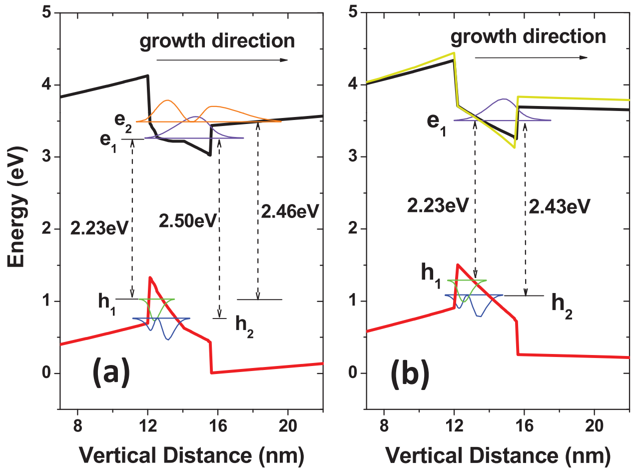

FIG. 6. (a) The energy band diagram and wave functions of the modified InGaN/GaN QWs. The modified QW structure is composed of 0.52 nm $In_{0.35}Ga_{0.65}N$ "wetting layer," 1.56 nm $In_{0.35\text{-}0.22}Ga_{0.65\text{-}0.78}N$ graded layers, and 1.56 nm $In_{0.22}Ga_{0.78}N$ layer along the growth direction. (b) The energy band diagram and wave functions of a 3.64 nm triangular QW with an $In_{0.33\text{-}0.23}Ga_{0.67\text{-}0.77}N$ graded layer. The energy band diagram of 3.64 nm $In_{0.30}Ga_{0.70}N$ rectangular QWs (yellow curve) is drawn for comparison. The carrier states are marked by "e" and "h," i.e., "e2" indicating the second quantized electron state and "h1" the first quantized hole state. Only the wave functions of e and h states providing contributions to the emission spectra are shown in the diagrams.

InGaN active layers along the growth direction) with interband transition energies close to that of the modified InGaN/GaN QWs was simulated and shown in Fig. 6(b). Compared with that of the rectangular InGaN/GaN QW structure (3.64 nm $In_{0.30}Ga_{0.70}N$, see the yellow curve), the PF-induced band bending for the triangular QWs (black curve) is reduced. The electron and hole states are marked by "e" and "h," i.e., "e2" the second quantized electron state and "h1" indicating the first quantized hole state (energy levels of heavy holes "hh" and light holes "lh" are indistinguishable with a graphical accuracy). Note that only the wave functions of e and h states providing contributions to the emission spectra are shown in the diagrams. The emission energy of the interband transitions from "e1" to "h1" and "e1" to "h2" are 2.23 eV (556 nm) and 2.43 eV (510 nm), respectively. According to the PL and EL spectra of the conventional triangular QWs, broad-band dual-wavelength emission was not observed.[42] Therefore, the minor contribution from the interband transition between "e1" and "h2" would not likely result in the dual-wavelength emission and spectral broadening in the emission spectra. The interband transition between "e1" and "h1" dominated in the emission spectrum of the conventional triangular QW structures.

For the modified InGaN/GaN QWs in Fig. 6(a), the PF-induced band bending is further reduced, leading to enhanced overlapping of the electron and hole wave functions for the first and second quantized carrier states. The involvement of the second quantized electron state "e2" in the interband transitions becomes possible due to the reduction in band bending and slight raise of the relative potential barrier at top of the QW. Since the situation of the modified InGaN QW is far from square QW, the selection rule of the interband transition between "e2" and "h1" being forbidden does not apply. The emission energy of the interband transitions from "e1" to "h1," "e2" to "h1," and "e1" to "h2" are 2.23 eV (556 nm), 2.46 eV (504 nm), and 2.50 eV (496 nm), respectively. Accordingly, the emission peak "P1" (and "p1") may be attributed to the interband transition from "e1" to "h1," whereas "P2" (and "p2") likely from "e2" to "h1" or from "e1" to "h2." As shown in Fig. 6(b) and the supplementary material,[42] contribution from the interband transition between "e1" and "h2" would not result in an extra peak in the PL and EL emission spectra. Consequently, in Fig. 5 for the PL and EL spectra of the modified InGaN/GaN QWs the emergence of the additional peak at higher emission energy is due to the major contribution from the enhanced interband transition between the excited electron state "e2" and the first quantized hole state "h1" to the emission spectra.

As shown in Fig. 6(a), the interband transition between "e2" and "h1" has stronger wave function overlap than that between "e1" and "h1." With the increase of injection current, the filling of excited electron state "e2" with electrons at high nonequilibrium carrier concentration in the well provides a major rise to the emission peak "p2," which interprets the evolution of the EL spectra with injection current and the emergence of the additional peak "p2" (and "P2") originating from the interband transition between "e2" and "h1." The decrease in the energy barriers on the p-side of each QW caused by the PF-induced band bending has been considered as one of the main reasons for the electron leakage (electrons overflow from the QW without being captured).[9–13] With the modified QW structure in this study, the band bending was further reduced by the energy band engineering as shown in Fig. 6(a); moreover, the involvement of the excited electron state "e2" provides more electron capture centers for radiative recombination at high carrier injection density; as a result, the carrier leakage or electron overflow loss from the InGaN active layers may be suppressed.

Figure 7 shows the simulated IQE as a function of injection current for the green-yellow LEDs with the conventional InGaN/GaN triangular QW structure and modified InGaN/GaN QW structure (see Fig. 6). The IQE is defined as the ratio of photons generated inside the QWs to the total electrons injected into the LED, which can be expressed as $\eta_{IQE} = \frac{I_{rad}}{(I_{rad}+I_{lost})}$, where I_{rad} denotes the carriers generating photons in the QW and I_{lost} the carriers lost to other processes without generating photons.[9] Great efforts were made to suppress the carrier loss in order to overcome the efficiency droop problem in nitride LEDs. As shown in Fig. 7, the maximum IQE for the conventional triangular QW structure and the modified QW structure is 0.60 and 0.91, respectively. With the increase of injection current to 20, 30, 50, and 100 mA, the IQE for the conventional triangular QWs drops to 0.26, 0.22, 0.17, and 0.12, respectively. In comparison, the IQE for the modified QWs is 0.82, 0.75, 0.60, and 0.41 for injection current at 20, 30, 50, and 100 mA, respectively. Obviously, the IQE for the modified InGaN/GaN QWs is much higher than that of the conventional triangular QWs due to the improvement in overlapping of the electron and hole wave functions by the energy band engineering using the modified active layer structure. Moreover, the

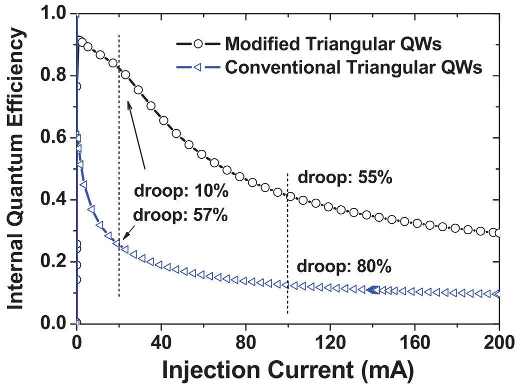

FIG. 7. Simulated IQE of the conventional InGaN/GaN triangular QWs and the modified InGaN/GaN QWs as a function of injection current showing the efficiency and droop improvements in the modified InGaN/GaN QWs.

efficiency droop for the conventional InGaN/GaN triangular QWs is 57% (20 mA), 63% (30 mA), 72% (50 mA), and 80% (100 mA), whereas the efficiency droop for the modified InGaN/GaN QWs is 10% (20 mA), 18% (30 mA), 34% (50 mA), and 55% (100 mA). Therefore, the luminous efficiency was improved and the efficiency droop was suppressed for the green-yellow LEDs using the modified InGaN/GaN QW structure. With increase of injection current, the EL intensity of the additional peak "p2" in Fig. 5(b) increases greatly, which interprets the suppression of the efficiency droop for the modified InGaN/GaN QWs. The efficiency and droop improvement, as discussed previously, are attributed to the enhanced overlapping of the electron and hole wave functions, reduction in PF-induced band bending, and enhanced interband transitions involving the excited quantized electron state by the energy band engineering.

IV. CONCLUSION

In summary, a modified InGaN active layer structure was proposed and achieved by indium pretreatment of the bottom GaN barriers and control of the growth temperature profile of the InGaN active layers. Various characterization techniques such as HR-TEM, HAADF-STEM, HR-XRD, XPS and PL combined with APSYS simulation were employed to investigate the modified InGaN/GaN QWs and to explore the origin of the luminescence properties experimentally and theoretically. The modified InGaN active layers were demonstrated to be of well defined profile and good interface abruptness, composed of 0.52 nm $In_{0.35}Ga_{0.65}N$ "wetting layer," 1.56 nm $In_{0.35\text{-}0.22}Ga_{0.65\text{-}0.78}N$ graded layers, and 1.56 nm $In_{0.22}Ga_{0.78}N$ layer along the growth direction. Broad-band dual-wavelength green-yellow emission at about 497 and 568 nm was observed, which may be applicable for monolithic or RGB white light sources. Energy band structures showed enhanced overlap of electron and hole wave functions, and enhanced interband transitions involving the excited electron state "e2" for the modified InGaN/GaN QWs compared with that of the conventional triangular QWs. With increase of injection current, major contribution of the interband transition between the excited electron state "e2" and the first quantized hole state "h1" to the emission spectra leads to the spectral broadening and broad-band dual-wavelength green-yellow emission. Further, the filling of excited electron state with electrons at high carrier injection density and the reduction in PF-induced band bending suppress the carrier leakage or electron overflow loss. APSYS simulation shows efficiency and droop improvements, which are attributed to the improvement in overlapping of electron and hole wave functions and the enhanced interband transitions involving the excited electron state for the modified InGaN active layers.

ACKNOWLEDGMENTS

This work was supported by the National Natural Science Foundation of China under Grant Nos. 60876008 and 61076091, and the Fundamental Research Funds for the Central Universities.

[1]C. F. Huang, T. Y. Tang, J. J. Huang, W. Y. Shiao, C. C. Yang, C. W. Hsu, and L. C. Chen, Appl. Phys. Lett. **89**, 051913 (2006).
[2]H. C. Lin, R. S. Lin, and J. I. Chyi, Appl. Phys. Lett. **92**, 161113 (2008).
[3]K. Y. Zang, S. J. Chua, J. H. Teng, N. S. S. Ang, A. M. Yong, and S. Y. Chow, Appl. Phys. Lett. **92**, 243126 (2008).
[4]Z. L. Fang, "Applications of surface/interface modification in group-III nitrides," in *Encyclopedia of Semiconductor Nanotechnology*, edited by A. Umar (American Scientific Publishers, Valencia, CA, 2012), Chap. 4, Vol. 1, pp. 1–57.
[5]K. P. O'Donnell, M. Auf der Maur, A. Di Carlo, K. Lorenz, and SORBET Consortium, Phys. Status Solidi (RRL) **6**, 49 (2012).
[6]Y. S. Lin, K. J. Ma, C. Hsu, S. W. Feng, Y. C. Cheng, C. C. Liao, C. C. Yang, C. C. Chou, C. M. Lee, and J. I. Chyi, Appl. Phys. Lett. **77**, 2988 (2000).
[7]T. Li, A. M. Fischer, Q. Y. Wei, F. A. Ponce, T. Detchprohm, and C. Wetzel, Appl. Phys. Lett. **96**, 031906 (2010).
[8]M. Feneberg and K. Thonke, J. Phys.: Condens. Matter **19**, 403201 (2007).
[9]J. Piprek, Phys. Status Solidi A **207**, 2217 (2010).
[10]G. Verzellesi, D. Saguatti, M. Meneghini, F. Bertazzi, M. Goano, G. Meneghesso, and E. Zanoni, J. Appl. Phys. **114**, 071101 (2013).
[11]M. H. Kim, M. F. Schubert, Q. Dai, J. K. Kim, E. F. Schubert, J. Piprek, and Y. Park, Appl. Phys. Lett. **91**, 183507 (2007).
[12]K. J. Vampola, M. Iza, S. Keller, S. P. DenBaars, and S. Nakamura, Appl. Phys. Lett. **94**, 061116 (2009).
[13]J. Piprek, R. Farrell, S. DenBaars, and S. Nakamura, IEEE Photonics Technol. Lett. **18**, 7 (2006).
[14]X. Ni, X. Li, J. Lee, S. Liu, V. Avrutin, Ü. Özgür, H. Morkoç, A. Matulionis, T. Paskova, G. Mulholland, and K. R. Evans, Phys. Status Solidi (RRL) **4**, 194 (2010).
[15]Y. C. Shen, G. O. Mueller, S. Watanabe, N. F. Gardner, A. Munkholm, and M. R. Krames, Appl. Phys. Lett. **91**, 141101 (2007).
[16]M. F. Schubert, S. Chhajed, J. K. Kim, E. F. Schubert, D. D. Koleske, M. H. Crawford, S. R. Lee, A. J. Fischer, G. Thaler, and M. A. Banas, Appl. Phys. Lett. **91**, 231114 (2007).
[17]X. Ni, Q. Fan, R. Shimada, Ü. Özgür, and H. Morkoç, Appl. Phys. Lett. **93**, 171113 (2008).
[18]Z. L. Fang, J. Y. Kang, and W. Z. Shen, Nanotechnology **20**, 045401 (2009).
[19]Z. L. Fang, J. Y. Kang, and W. Z. Shen, J. Phys. Chem. C **112**, 17652 (2008).
[20]E. H. Park, D. N. H. Kang, I. T. Ferguson, S. K. Park, and T. K. Yoo, Appl. Phys. Lett. **90**, 031102 (2007).
[21]M. F. Schubert, J. Xu, J. K. Kim, E. F. Schubert, M. H. Kim, S. Yoon, S. M. Lee, C. Sone, T. Sakong, and Y. Park, Appl. Phys. Lett. **93**, 041102 (2008).
[22]M. H. Kim, W. Lee, D. Zhu, M. F. Schubert, J. K. Kim, E. F. Schubert, and Y. Park, IEEE J. Sel. Top. Quantum Electron. **15**, 1122 (2009).
[23]D. F. Feezell, M. C. Schmidt, S. P. Denbaars, and S. Nakamura, MRS Bull. **34**, 318 (2009).
[24]F. Scholz, T. Wunderer, B. Neubert, M. Feneberg, and K. Thonke, MRS Bull. **34**, 328 (2009).

[25]M. Funato, K. Hayashi, M. Ueda, Y. Kawakami, Y. Narukawa, and T. Mukai, Appl. Phys. Lett. **93**, 021126 (2008).
[26]Z. L. Fang, Y. X. Lin, and J. Y. Kang, Appl. Phys. Lett. **98**, 061911 (2011).
[27]Z. H. Wu, T. Tanikawa, T. Murase, Y.-Y. Fang, C. Q. Chen, Y. Honda, M. Yamaguchi, H. Amano, and N. Sawaki, Appl. Phys. Lett. **98**, 051902 (2011).
[28]H. P. Zhao, R. A. Arif, and N. Tansu, IEEE Sel. Top. Quantum Electron. **15**, 1104 (2009).
[29]H. P. Zhao, G. Y. Liu, X. H. Li, G. S. Huang, J. D. Poplawsky, S. T. Penn, V. Dierolf, and N. Tansu, Appl. Phys. Lett. **95**, 061104 (2009).
[30]C. T. Liao, M. C. Tsai, B. T. Liou, S. H. Yen, and Y. K. Kuo, J. Appl. Phys. **108**, 063107 (2010).
[31]Y. X. Lin and Z. L. Fang, Appl. Phys. A **103**, 317 (2011).
[32]Y. A. Chang, J. Y. Chang, Y. T. Kuo, and Y. K. Kuo, Appl. Phys. Lett. **100**, 251102 (2012).
[33]S. H. Park, D. Ahn, B. H. Koo, and J. W. Kim, Appl. Phys. Lett. **95**, 063507 (2009).
[34]F. Wu, W. Tian, W. Y. Yan, J. Zhang, S. C. Sun, J. N. Dai, Y. Y. Fang, Z. H. Wu, and C. Q. Chen, J. Appl. Phys. **113**, 154505 (2013).
[35]Z. L. Fang, J. Y. Kang, W. J. Huang, H. T. Sun, M. Lu, J. F. Kong, and W. Z. Shen, J. Phys. Chem. C **112**, 4925 (2008).
[36]Z. L. Fang, D. Q. Lin, J. Y. Kang, J. F. Kong, and W. Z. Shen, Nanotechnology **20**, 235401 (2009).
[37]S. H. Han, D. Y. Lee, S. J. Lee, C. Y. Cho, M. K. Kwon, S. P. Lee, D. Y. Noh, D. J. Kim, Y. C. Kim, and S. J. Park, Appl. Phys. Lett. **94**, 231123 (2009).
[38]See http://www.crosslight.com for APSYS2012 by Crosslight Software Inc., Burnaby, Canada.
[39]S. Pereira, Thin Solid Films **515**, 164 (2006).
[40]S. Pereira, K. P. O'Donnell, and E. Alves, Adv. Funct. Mater. **17**, 37 (2007).
[41]*Nitride Semiconductor Devices: Principles and Simulation*, edited by J. Piprek (Wiley-VCH, Berlin, 2007), Chap. 14.
[42]See supplementary material at http://dx.doi.org/10.1063/1.4863208 for PL and EL data of the conventional InGaN/GaN triangular quantum wells.